splittings,[19-21] Q^F_{eff} values (in G) were calculated for four perfluoroaromatic radical cations and the results are given in Table I. Bearing in mind that appreciable errors may be introduced in the computation for positions of low spin density, the spread of calculated Q^F_{eff} values is remarkably small and most of them are clustered between 90 and 104 G. Other authors have made estimates of 93.1 G[21] and 107.4 G[19] for this parameter from data on both perfluorinated and partially fluorinated aromatic radical cations.

Also included in Table I are the results of this work on $C_8F_8^-$ which yields a Q^F_{eff} value of 94.2 G. The good agreement between this value and the results derived from the perfluoroaromatic radical cations is striking. Moreover, a recent study of the neutral C_5F_5 radical indicates a very similar value of 98.2 G,[22] further supporting the idea that Q^F_{eff} is sensibly constant for electron-deficient aromatic π radicals, irrespective of the electric charge on the radical. The isostructural character of these species is also confirmed by the fact that their isotropic g values (Table II) are grouped in a narrow range with a small positive shift from the free-spin value. We conclude, therefore, that the ESR parameters for $C_8F_8^-$ are strongly supportive of a planar aromatic radical.

(22) Chen, T.; Graf, F.; Günthard, Hs. H. *Chem. Phys.* **1983**, *75*, 165. These authors report an isotropic fluorine hyperfine coupling $a_F(5)$ of 16.0 G for C_5F_5 at 170 K. Combining this result with an average spin population of 0.163 in each of the carbon $2p_z$ orbitals, as deduced from an INDO calculation, a Q^F_{eff} of 98.2 G is obtained.

Acknowledgment. D.M.L. wishes to thank Professor Josef Michl (University of Utah) for suggesting the ultimately successful approach to the C_8F_8 radical anion and for providing facilities for the initial attempts to observe it in matrix isolation. He also thanks the National Science Foundation and the donors of the Petroleum Research Fund, administered by the American Chemical Society, for generous financial support. The work at the University of Tennessee was supported by the Division of Chemical Sciences, Office of Basic Energy Sciences, U.S. Department of Energy (Document No. DOE/ER/02968-149).

Registry No. Octafluorocyclooctatetraene radical anion, 88211-63-6.

Nuclear Spin Relaxation and Ring-Current Shifts in Chlorophyll Dimers

R. P. H. Kooyman[†] and T. J. Schaafsma*

Contribution from the Department of Molecular Physics, Agricultural University, de Dreijen 11, 6703 BC Wageningen, The Netherlands. *Received September 13, 1982*

Abstract: ^1H spin–lattice relaxation (SLR) times and chemical shifts of various protons in chlorophyll *a* monomer, the "special pair" (SP) dimer and the (Chl *a*)$_2$ dimer have been determined at 100 MHz. The SLR times can be related to the geometry of the particular dimer by applying a rotational diffusion model. Due to the limited number of protons suitable for SLR experiments, this comparative study provides a check on previously proposed dimer structures but cannot define entirely new geometries. An independent check on these geometries is provided by the experimental ring-current shifts. Calculations employing either SLR data or ring-current shifts yield very similar geometries for both types of dimers. In particular, the signs and relative magnitudes of the ring-current shifts turn out to be sensitive to the dimer structure. Both macrocycles in the (Chl *a*)$_2$ dimer are found to be perpendicular, corresponding to a rotation over the Eulerian angles (90°, 90°, 135°); their centers are displaced by the vector (7.5, −0.65, 0) (Å) in an axis system fixed to one of the monomers; the rotational diffusion tensor elements are $D_{xx} = 0.6$, $D_{yy} = 3$, $D_{zz} = 2$ ($\times 10^9$ s^{-1}). Experimental results for the ethanol-linked SP dimer confirm the Shipman–Katz geometry, defined by the relative translation (7.7, −0.13, 3.6) (Å) and rotation (0°, 180°, 180°); the rotational diffusion tensor elements are $D_{xx} = 0.5$, $D_{yy} = 0.5$, $D_{zz} = 3$ ($\times 10^9$ s^{-1}). For both dimers, the average diffusion constant is found to be approximately half that of the monomer, as expected. However, the relative magnitudes of the separate components of the rotational diffusion tensor of both dimers cannot be simply rationalized by an anisotropic hydrodynamic model.

During the last decade various chlorophyll species in vivo and in vitro have been extensively studied.[1-7] The occurrence of various forms of chlorophyll in vitro depends on the nature of their environment and has provided proposals for the structure of chlorophyll complexes in vivo.[4a,b] In particular the Chl *a* dimer (Chl *a*)$_2$ and the Chl *a* "special pair" (SP) (Chl *a*·L)$_2$, where L is a ligand (e.g., H_2O), have been suggested to be important in photosynthesis.[4a,b]

To assess to what extent these complexes may serve as models for the photosynthetic apparatus, it is important to know their geometry as precisely as possible, since that will largely determine such properties as the absorption spectrum and ionization potential, which make some chlorophyll complexes suited for their role in photosynthesis.

For the SP dimer, IR[8] and ESR[9] data suggest that two Chl *a* molecules are held in a plane-parallel orientation via two ligands with both electron-donor and electron-acceptor properties.[4a,b,10] From CD[11] and NMR[12] studies it was concluded that the two macrocycles in (Chl *a*)$_2$ are ~40° tilted relative to each other, but this geometry has not generally been accepted.[13]

[†]Present address: Department of Biophysics, Princetonplein 5, State University of Utrecht, The Netherlands.

(1) Seely, G. R. In "Primary Processes of Photosynthesis"; Barber, J., Ed.; Elsevier: Amsterdam, 1977.
(2) Sauer, K. In "Bioenergetics of Photosynthesis"; Govindjee, Ed.; Academic Press: New York, 1975; Chapter 3 and references cited therein.
(3) Fenna, R. E.; Matthews, B. W., ref 4b, pp 170–182.
(4) (a) Katz, J. J.; Shipman, L. L.; Norris, J. R. *Excerpta Med. Ciba Found. 61 (new Ser.)* **1979**. (b) Katz, J. J.; Shipman, L. L. *Brookhaven Symp. Biol.* **1976**, *28*, 17.
(5) Krasnovskii, A. A.; Bystrova, M. I. *Biosystems* **1980**, *12*, 181.
(6) Hoshino, M.; Ikehara, K.; Imamura, M.; Seki, H.; Hama, Y. *Photochem. Photobiol.* **1981**, *34*, 75.
(7) Yuen, M. J.; Shipman, L. L.; Katz, J. J.; Hindman, J. C. *Photochem. Photobiol.* **1982**, *36*, 211.
(8) (a) Cotton, T. M.; Loach, P. A.; Katz, J. J.; Ballschmiter, K. *Photochem. Photobiol.* **1978**, *27*, 735. (b) Cotton, T. M. Ph.D. Thesis, Northwestern University, Evanston, IL, 1977.
(9) Kooyman, R. P. H.; Schaafsma, T. J.; Kleibeuker, J. F. *Photochem. Photobiol.* **1977**, *26*, 235.
(10) (a) Fong, F. K. *Appl. Phys.* **1975**, *6*, 151. (b) Fong, F. K. "Theory of Molecular Relaxation: Applications in Chemistry and Biology; Wiley-Interscience: New York, 1975; Chapter 9. (c) Fong, F. K.; Koester, V. J. *Biochim. Biophys. Acta.* **1976**, *423*, 52.

0002-7863/84/1506-0551$01.50/0

Following similar high-resolution NMR studies on small molecules,[14-17] we investigated the solution structure of (Chl a)$_2$ and (Chl a·L)$_2$ by ^{1}H spin–lattice relaxation experiments. A comparison of experimental and predicted ring-current chemical shifts for Chl a and its dimers provides additional and independent support for the proposed structures.

Nuclear Spin Relaxation and Molecular Structure

For a discussion of the relation between nuclear relaxation data and molecular structure for Chl a and its dimers, we focus on the spin–lattice (T_1) relaxation process and assume the rotational diffusion model to be valid. For this model the elements of the rotational diffusion tensor $\boldsymbol{D}$ describing the anisotropic molecular reorientation can be derived from the relaxation times of an appropriate set of nuclei in the molecule.[18,19]

In the absence of internal mobility, T_1 of a $I = {}^1/_2$ nucleus i due to intramolecular dipole–dipole interaction with $n-1$ other nuclei is given by[19]

$$\frac{1}{{}_iT_1} = C\sum_{j\neq i} f(\Omega_j, \boldsymbol{D})\frac{1}{r_{ij}^6} \equiv \sum_j g(\Omega_j, \boldsymbol{D}, r_{ij}) \quad (i, j = 1, ..., n) \quad (1)$$

where f is a function of tensor $\boldsymbol{D}$ and the polar angles $\Omega_j \equiv (\phi_j, \theta_j)$ of nucleus j with respect to a molecular frame of reference diagonalising tensor $\boldsymbol{D}$; C is a nuclear constant and r_{ij} is the internuclear distance; f has the property

$$f(\Omega, \lambda\boldsymbol{D}) = (1/\lambda)f(\Omega, \boldsymbol{D}) \quad (2)$$

where λ is a scalar. Only *relative* values of the components of tensor $\boldsymbol{D}$ are needed to elucidate the molecular structure. Therefore ${}_iT_1$ can be scaled by $\langle T_1\rangle$, the average of the T_1 values.[20] Combining eq 1 and 2 yields the result

$$\frac{{}_iT_1}{\langle T_1\rangle} = \frac{\sum_i\sum_{j\neq i} g(\Omega_j, \lambda\boldsymbol{D}, r_{ij})}{n\sum_{j\neq i} g(\Omega_j, \lambda\boldsymbol{D}, r_{ij})} = \frac{\sum_i\sum_{j\neq i} g(\Omega_j, \boldsymbol{D}, r_{ij})}{n\sum_{j\neq i} g(\Omega_j, \boldsymbol{D}, r_{ij})}$$
$$(i, j = 1, ..., n) \quad (3)$$

i.e., independent of λ. From the functions g, containing the structural information, and using eq 3, we now are able to calculate relative T_1 values and fit these to the experimental T_1 values with the elements of tensor $\boldsymbol{D}$ as adjustable parameters. The resulting scaled diffusion tensors $\boldsymbol{D}_i'$ and the actual tensor $\boldsymbol{D}$ are related by

$$\boldsymbol{D} = \lambda\boldsymbol{D}' \quad (4)$$

with $\lambda = \langle T_1\rangle_{\text{exptl}}/\langle T_1\rangle_{\text{calcd}}$. For a dimer composed of two fast exchanging identical monomers, T_1 is given by

$$\frac{1}{{}_iT_1} = \frac{1}{2}\left[\frac{1}{{}_iT_1^{(1)}} + \frac{1}{{}_iT_1^{(2)}}\right] \quad (5)$$

where both $1/T_1^{(1)}$ and $1/T_1^{(2)}$ are given by an expression of the type

$$1/{}_iT_1 = \sum_j g(\Omega_j, \boldsymbol{D}, r_{ij}) + \sum_j g(\Omega_j', \boldsymbol{D}, r_{ij}') \quad (6)$$

In eq 6 the first term describes the relaxation caused by nuclei in the same subunit as the observed nucleus; the second term contains the contribution from nuclei of the other subunit.

Of course, eq 5 and 6 are not suitable to apply to a molecule with a completely unknown structure due to the large number of unknown geometrical parameters, r_{ij}, θ_i, ϕ_i. However, if the monomeric structure is known, then the dimer structure is completely defined by three rotations over Eulerian angles $\Omega = (\alpha, \beta, \gamma)$ and three translations $\vec{V} = (x, y, z)$ of one monomer relative to the other.

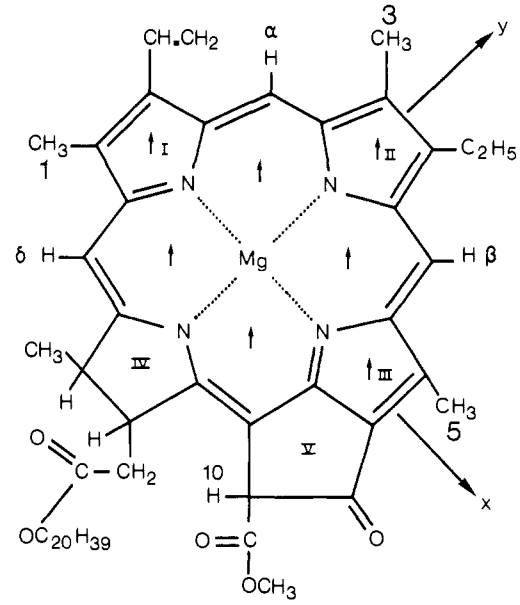

Figure 1. Molecular structure of chlorophyll a. The position of equivalent magnetic dipoles has been indicated by arrows; relevant protons have been conventionally labeled. The molecular frame of reference is defined by the axes x and y; z is perpendicular to the molecular plane.

Molecular Structure of Chlorophyll Dimers. The X-ray structure[21] of ethyl chlorophyllide a has been used for the interatomic distances within a Chl a monomer. Equation 4 only pertains to nuclei without internal mobility; for Chl a, there are only four such protons (denoted by α, β, δ, and 10 in Figure 1) that have a reasonable intensity in the NMR spectrum, and thus are suitable for relaxation studies. From the monomeric atomic coordinates, those of a dimer were generated by applying a translation $\vec{V}$ and a rotation over the Eulerian angles $\Omega = \alpha, \beta$ and γ on all monomeric atomic coordinates and combining the original and transformed coordinates. The geometry of a particular Chl a dimer is found for those translations $\vec{V}$ and rotations Ω that yield an optimum fit between the experimental and calculated T_1 values by using eq 3 and minimizing

$$\epsilon = \sum_i\left[\frac{({}_iT_1)_{\text{calcd}}}{\langle T_1\rangle_{\text{calcd}}} - \frac{({}_iT_1)_{\text{exptl}}}{\langle T_1\rangle_{\text{exptl}}}\right]^2 \quad (7)$$

Molecular Frame of Reference. Equations 1–4 are only valid in an axis system diagonalizing tensor $\boldsymbol{D}$. For a totally asymmetric molecule such as Chl a, the proper choice of the diffusion axis system is not a priori obvious.[19] Approximating Chl a and its dimers as solid bodies with a uniform mass distribution, the diffusion- and inertial-axis systems are assumed to be approximately coincident.[22] This assumption can in principle be verified independently by ^{2}H relaxation measurements.[18,19] Unfortunately, T_1 values of perdeuterated Chl a were inconclusive, because in Chl a there are no four rigid, nonequivalent ^{2}H nuclei with sufficient NMR amplitude.

The agreement between the dimer geometries derived from SLR and chemical shifts provides an a posteriori justification for the assumption of coinciding inertial and diffusion axes.

Proton Chemical Shifts and Molecular Structure

An alternative way to study molecular structure is to measure and calculate the ring-current chemical shifts of individual nuclei

(11) Houssier, C.; Sauer, K. *J. Am. Chem. Soc.* **1970**, *92*, 779.
(12) Katz, J. J.; Norris, J. R. *Curr. Top. Bioeng.* **1973**, *5*, 41.
(13) Shipman, L. L. *J. Phys. Chem.* **1977**, *81*, 2180.
(14) Wallach, D.; Huntress, W. T. *J. Chem. Phys.* **1969**, *50*, 1219.
(15) Vold, R. L.; Vold, R. R.; Canet, D. *J. Chem. Phys.* **1977**, *66*, 1202.
(16) Bovée, W. M. M. J. Ph.D. Thesis, University of Delft, 1975.
(17) Pedersen, E. J.; Vold, R. R.; Vold, R. L. *Mol. Phys.* **1978**, *35*, 997.
(18) Huntress, W. T. *Adv. Magn. Reson.* **1970**, *4*, 1.
(19) Huntress, W. T. *J. Chem. Phys.* **1968**, *48*, 3524.
(20) By use of eq 3, the problem of a priori scaling of tensor $\boldsymbol{D}$ can be circumvented; simultaneously, nongeometrical effects on tensor $\boldsymbol{D}$, such as the influence of temperature, are eliminated.

(21) Chow, H. C.; Serlin, R.; Strouse, C. E. *J. Am. Chem. Soc.* **1975**, *97*, 7230.
(22) Brenner, H. *Chem. Eng. Sci.* **1964**, *19*, 519.

Table I. Chemical Shifts (δ) and Ring-Current Shifts ($\Delta\delta$) in Chlorophyll[a]

	monomer[b]			dimer[c]			SP[c,d]		
		$\Delta\delta$(mono)			$\Delta\delta$(dimer) − $\Delta\delta$(mono)			$\Delta\delta$(SP) − $\Delta\delta$(mono)	
proton[e]	δ	exptl	calcd[f]	δ	exptl	calcd	δ	exptl	calcd
α	9.36	4.24	4.42	9.20	−0.16	−0.03	9.87	0.51	0.20
β	9.70	4.58	4.42	9.40	−0.30	−0.23	9.90	0.20	−0.30
δ	8.54	3.42	3.57	8.22	−0.32	−0.06	8.87	0.33	0.19
10	6.17		1.84	~4.70[g]	−1.47	−0.91	~8	1.83	0.70
1	3.33	1.83	1.90	3.31	−0.02	−0.16			
3	3.27	1.77	2.01	3.22	−0.05	0.04			
5	3.58	2.08	1.97	2.80	−0.78	−0.55			

[a] δ relative to Me_4Si; $\Delta\delta$ relative to pyrrole,[28] calculated according to $(\Delta\delta)_{Chl} = \delta_{Chl} - \delta_{pyrrole} + (\Delta\delta)_{pyrrole}$. [b] Determined at 360 MHz. [c] Determined at 100 MHz. [d] Experimental values of δ and $\Delta\delta$ have been corrected for the presence of $(Chl\ a)_2$ dimer (see text, eq 12); the calculated results are those for the Shipman–Katz structure. [e] Numbering according to Figure 1. [f] Results for $\mu_H = 21 \times 10^{-3}$ nm^3, $\mu_P = 18 \times 10^{-3}$ nm^3 (see eq 8). [g] Value obtained by extrapolating to zero concentration of methanol as ligand, following ref 32.

in the molecule.[23-27] For porphyrins and chlorophyll derivatives the macrocycle is divided into a number of π-electron current loops with equivalent dipoles placed at the center of each loop[24,26] (see Figure 1), yielding fairly good agreement between calculated and experimental chemical shifts.[28a,b]

The experimental chemical shifts for Chl *a* monomer and dimers are appreciably different (Table I) and contain information about the geometry of the dimers. We have employed the method of Abraham et al.[28a,b] to relate the ring-current chemical shifts in Chl *a* dimers to their geometry.

For the Chl *a* monomer the ring-current shift of a proton *N* is given by[28a,29]

$$\Delta\delta(N) = \sum_{i=1}^{8}\mu_H[1 - 3(z_{Ni}/r_{Ni})^2]/r_{Ni}^3 + \sum_{j=1}^{6}\mu_P[1 - 3\,(z_{Nj}/r_{Nj})^2]/r_{Nj}^3 \quad (8)$$

where r_{Ni} and r_{Nj} are the distances from proton N to the equivalent dipoles *i*, placed at a distance *z* above and below the hexagons of Figure 1 and, similarly, to the dipoles *j*, placed above and below the pyrrole rings, respectively; z_{Ni} and z_{Nj} are the *z* coordinates of the vectors connecting proton N and the dipoles *i* and *j*, respectively (see Figure 1). μ_H and μ_P (in nanometer cubed) denote the magnitude of the dipole moments placed in the hexagons and pyrrole rings;[29] distances are in nanometers and $\Delta\delta$(N) in parts per million.

For a dimer made from two identical monomers, the set of magnetic dipole vectors $\{\vec{\mu}_1\}$, representing the ring currents in molecule 1, and a similar set of vectors $\{\vec{\mu}_2\}$ in molecule 2 are related by the transformation $\{\vec{\mu}_2\} = \boldsymbol{R}\{\vec{\mu}_1\}$, where $\vec{R}$ includes both translation and rotation. The coordinates $\vec{r} = (N_x, N_y, N_z)$ of an equivalent nucleus in each of both molecules are related by $\vec{r}_{N2} = \boldsymbol{R}\vec{r}_{N1}$. The ring-current shift of a particular proton in one-half of the dimer contains contributions from the magnetic dipoles within the same half as well as from those in the other half of the dimer. If both halves are indistinguishable on the NMR time scale, due to fast exchange, then the net ring-current shift is given by

$$\Delta\delta(N)_{dimer} = \Delta\delta(N_i)_{\{\vec{\mu}_i\}} + \tfrac{1}{2}\sum_{i,j}\Delta\delta(N_i)_{\{\vec{\mu}_j\}} \qquad (i \neq j = 1, 2) \quad (9)$$

where $\Delta\delta(N_i)_{\{\vec{\mu}_j\}}$ denotes the ring-current shift of a particular proton of monomer *i*, due to the magnetic dipoles $\{\mu_j\}$, associated with monomer *j*. The first and last two terms in eq 9 contain the monomer and dimer contributions, respectively, to the net ring-current shift. The ring-current shift of a particular proton can now be calculated by applying eq 8 to each of the terms in eq 9 after a second transformation that makes the dipoles in molecule 2 parallel to the *z* axis. Denoting the position of dipole $\vec{\mu}_2$ by $\vec{r}_\mu$ and that of proton *N* by $\vec{r}_N$, and the rotational part of tensor $\boldsymbol{R}$ by tensor $\boldsymbol{R}_{rot}$, the new vectors $(\vec{r}_N)' = (\boldsymbol{R}_{rot})^{-1}(\vec{r}_N - \vec{r}_\mu)$ and $(\vec{r}_\mu)' = (0, 0, 0)$ represent the same relative positions of the proton *N* and the dipole $\vec{\mu}_2$ as $\vec{r}_N$ and $\vec{r}_\mu$ (see Figure 2). The last term in eq 9 can now be evaluated by eq 8 after applying this transformation to each dipole in the set $\{\vec{\mu}_2\}$. The remaining terms in eq 9 can be calculated by applying eq 8 without the aforementioned transformation (see Figure 2).

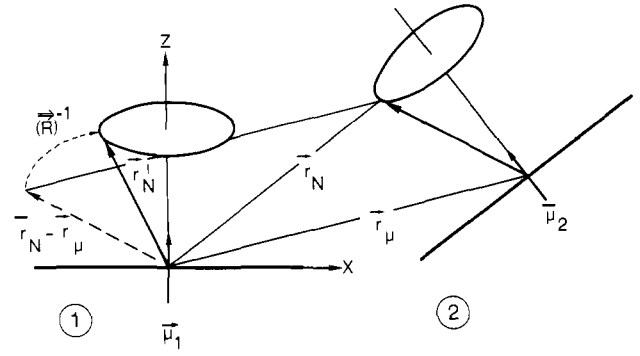

Figure 2. Transformation of the position of nucleus *N* relative to $\vec{\mu}_2$ in molecule 2 to a position $\vec{r}_N'$ relative to the origin in molecule 1. Molecules 1 and 2 are represented by heavy lines. The $\{x, y, z\}$ axis system is fixed to molecule 1; in the origin the transformed $\vec{\mu}_2$ is parallel to the *z* axis.

Equation 8 was calibrated for Chl *a* by using pyrrole as a reference compound.[29] We have determined those values of μ_H and μ_P that produce an optimum fit between calculated and experimental ring-current shifts for the Chl *a* monomer. The positions of the 14 equivalent dipoles were kept constant; each loop contained two dipoles in its center, at $z = \pm 0.64$ nm.

Ring-current shifts in Chl *a* dimers were calculated, using the monomer values of μ_H and μ_P and generating the dimer as described before. By varying the dimer geometry, an optimum fit was found between the calculated and experimental ring-current shifts of the protons marked in Figure 1 (see Table I).

Experimental Section

Sample Preparation. Three types of samples were prepared: (1) Chl *a* in deuterated acetone, in which Chl *a* is monomeric;[8a,b] (2) Chl *a* in deuterated chloroform, in which Chl *a* mainly exists in the dimeric form

(23) Emsley, J. W.; Feeney, J.; Sutcliffe, L. H. "High Resolution Nuclear Magnetic Resonance Spectroscopy"; Pergamon Press: Oxford, 1968; Vol. 2.
(24) Pople, J. A. *J. Chem. Phys.* **1956**, *24*, 1111.
(25) Johnson, C. E.; Bovey, F. A. *J. Chem. Phys.* **1958**, *29*, 1012.
(26) Abraham, R. J. *Mol. Phys.* **1961**, *4*, 145.
(27) Ditchfield, R. "Specialist Periodical Report on NMR Spectroscopy"; Chemical Society: London, 1976; Vol. 5, Chapter 1.
(28) (a) Abraham, R. J.; Fell, S. C. M.; Smith, K. M. *Org. Magn. Reson.* **1977**, *9*, 367. (b) Abraham, R. J.; Smith, K. M.; Goff, D. A.; Lai, J. *J. Am. Chem. Soc.* **1982**, *104*, 4332.
(29) Abraham et al.[28b] have applied a refined equivalent dipole model to chlorophyll derivatives, including the effects of the ring V keto group and the saturated ring IV on the ring-current chemical shifts, resulting in a better prediction of the shifts of the NH protons. Since the shifts of the other protons remain essentially unchanged and we are only interested in the shifts of peripheral protons, it is appropriate to use the double-dipole model[28a] yielding eq 8. By adjusting μ_H and μ_P, we implicitly account for the presence of the ring keto group and the saturated ring IV. As expected, the values of μ_H and μ_P, producing an optimum fit for the Chl *a* monomer, come out somewhat lower than those used in Abraham's refined model.[28b]
(30) Strain, H. H.; Svec, W. A. in "The Chlorophylls"; Vernon, L. P., Seely, G. R., Eds.; Academic Press: New York, 1966; Chapter 2.

Table II. Proton SLR Times (s) for Chl *a* Monomer and Dimers[a]

proton	Chl *a* monomer	$(Chl\ a)_2$	Chl *a* SP[b]
α	1.07 ± 0.06	0.43 ± 0.04	0.31 ± 0.05
β	0.95 ± 0.06	0.40 ± 0.04	0.18 ± 0.03
δ	0.92 ± 0.06	0.32 ± 0.03	0.22 ± 0.04
10	1.45 ± 0.09	0.55 ± 0.05	0.41 ± 0.07

[a] 100 MHz. Errors are quoted as standard deviations and are the rms sums of estimated instrument reproducibility and standard deviation of exponential fit. For sample 3 an additional error is introduced by the error in the equilibrium constant k_2. [b] Corrected for the presence of $(Chl\ a)_2$ in the sample (see text, eq 12).

$(Chl\ a)_2$;[8a,b] (3) Chl *a* in deuterated toluene/ethanol, which at low temperature ($T \sim 260$ K) is partly in the "SP" form $(Chl\ a{\cdot}EtOH)_2$.[8a,b]

Chl *a* was extracted from spinach leaves and purified according to standard procedures.[29] Purity was checked by absorption spectrophotometry and TLC. Milligram quantities of pure Chl *a* were extensively dried at 10^{-5} torr and ~60 °C. Fully deuterated solvents (Merck) were dried over 4-Å molecular sieves (Union Carbide) according to the procedure of Cotton[8a,b] and thoroughly degassed. Preparations were carried out in a nitrogen-purged drybox. Samples with 0.01–0.8 M Chl *a* concentration were contained in NMR tubes, sealed immediately after preparation. Sample 3 was prepared according to Cotton's procedure,[8a,b] with a molar Chl *a*/ethanol ratio of ~0.25. Its absorption spectrum, employing a 25-μm path length microcell (Beckman Instruments), exhibits a band at 700 nm at ~250 K, indicating the presence of $(Chl\ a{\cdot}EtOH)_2$.[8a,b]

NMR Experiments. Except for sample 3, all NMR experiments were carried out at room temperature in 5-mm sample tubes. Sample 3 was studied at $T = 260$ K. ^1H experiments were carried out with samples 1, 2, and 3 on a Varian XL-100 NMR spectrometer at 100 MHz and at 360 MHz on a Bruker Supercon spectrometer. T_1's were determined for the protons H_α, H_β, H_δ, and the single proton H_{10} (Figure 1) by inversion recovery and using a nonlinear least-squares fit.[31]

For the samples 2 and 3 an equilibrium exists between various forms of Chl *a*. In the limit of fast chemical exchange between two such species, A and B, the observed value of $(T_1)^{-1}$ for a given nucleus is given by

$$(T_{1(obsd)})^{-1} = f_A(T_1^A)^{-1} + (1 - f_A)(T_1^B)^{-1} \quad (10)$$

where $f_A = [A]/([A] + [B])$ and T_1^A and T_1^B are the SLR times of that nucleus in the separate species.

For sample 2 the equilibrium constant was determined[32] for the reaction

$$(Chl\ a)_2 + 2L \underset{}{\overset{k_1}{\rightleftharpoons}} 2Chla{\cdot}L \ (L = methanol) \quad (11)$$

For sample 3, the equilibrium has the form[8a,b]

$$(Chl\ a)_2 + 2L \overset{k_2}{\rightleftharpoons} (Chl\ a{\cdot}L)_2 \quad (12)$$

To identify the resonances of Chl *a* and $(Chl\ a)_2$ for SLR experiments, we used the assignments of Katz et al.[33] and Denniss et al.[34] The presence of significant amounts of polymeric species is very unlikely since dimer SLR times for sample 2 did not change upon further dilution to 10^{-3} M.

Results

The chemical shifts for monomeric Chl *a* (sample 1), the $(Chl\ a)_2$ dimer (sample 2), and Chl *a* SP (sample 3) have been collected in Table I. For the $(Chl\ a)_2$ dimer there is good agreement with previously reported values.[33] For the monomer, there are systematic differences with reported chemical shifts.[33] We note, however, that Katz et al.[33] have used somewhat higher chlorophyll concentrations for their NMR measurements.

For the total Chl *a* concentration ($C_0 \simeq 5 \times 10^{-2}$ M) in the $(Chl\ a)_2$ sample and the equilibrium constant $k_1 \simeq 40$ L/mol (eq 11), the total ligand concentration L_0 was determined from the positions of methyl resonances in sample 2.[32] From the resulting ratio $L_0/C_0 \simeq 0.35$, we conclude that more than 90% of the chlorophyll is in the dimeric form; therefore, no corrections have been made to the chemical shifts and T_1 values in Tables I and II.

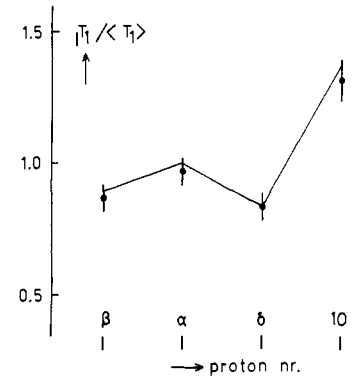

Figure 3. Experimental and calculated T_1 values of the protons α, β, δ, and 10 in the Chl *a* monomer. (●) observed; (—) calculated.

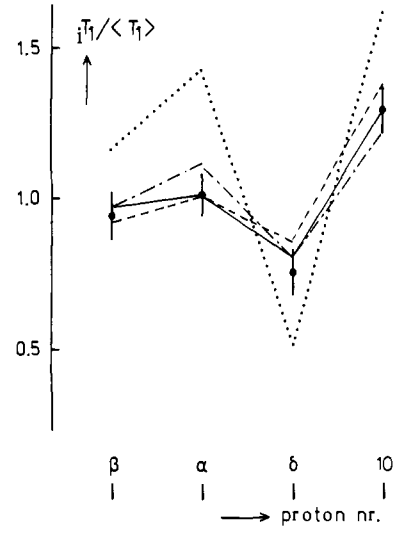

Figure 4. Results of T_1 calculations for some geometries of the $(Chl\ a)_2$ dimer: (···) geometry according to Katz et al.;[12] (··· $\vec{V} = (7.5, -0.65, 0)$, $\vec{\Omega} = (90, 90, 90)$; (—) $\vec{V} = (7.5, -0.65, 0)$, $\vec{\Omega} = (90, 90, 135)$; (- - -) $\vec{V} = (7.5, -0.65, 0)$, $\vec{\Omega} = (90, 90, 120)$; (●) observed.

For Chl *a* SP (sample 3), however, $k_2 = 15$ L/mol^2 at 260 K[8a,b] and the total Chl concentration $C_0 \simeq 8 \times 10^{-2}$ M and [ethanol] ≃ 0.3 M; the ratio $[SP]/C_0$ is calculated to be ≃0.23. In consequence, the chemical shifts and T_1 values determined for sample 3 do not reflect those of "pure" Chl *a* SP. Therefore, we determined shifts and T_1 values at $T = 260$ K for $(Chl\ a)_2$[8a,b] in dry toluene; from eq 10, the T_1 values and, similarly, the chemical shifts of "pure" SP have been calculated.

Since the multiplets of the ^1H NMR spectrum collapse into singlets in the ^2H NMR spectrum, we have used the ^2H spectrum at 61.4 MHz of monomeric Chl *a* as a check on the assignments of the proton resonances in Table I.

The assignment of H_α, H_β, H_δ, and H_{10} resonances of Chl *a* SP is based on previous results on porphyrins,[33,35] which indicate that the low-field resonances α, β, and δ correspond to methine protons. In order to determine which of the resonances at ~6 ppm corresponds to proton 10, we have determined SLR times for all resonances in that region. All SLR times were found to be about the same, except for one, which was ~3 times longer. In view of the relatively isolated position of proton 10, we assign this resonance to this proton.

(31) Provencher, S. W. *J. Chem. Phys.* **1976**, *64*, 2772.
(32) Katz, J. J.; Strain, H. H.; Leussing, D. L.; Dougherty, R. C. *J. Am. Chem. Soc.* **1968**, *90*, 784.
(33) (a) Katz, J. J.; Dougherty, R. C.; Boucher, L. J. ref 30, Chapter 7. (b) Katz, J. J.; Shipman, R. L.; Cotton, T. M.; Janson, T. R. In "The Porphyrins"; Dolphin, D., Ed.; Academic Press: New York, 1978; Chapter 9.
(34) Denniss, I. S.; Sanders, J. K. M.; Waterton, J. C. *J. Chem. Soc., Chem. Commun.* **1976**, 1049.
(35) Abraham, R. J.; Burbridge, P. A.; Jackson, A. H.; Kenner, G. W. *Proc. Chem. Soc.* **1963**, 134.

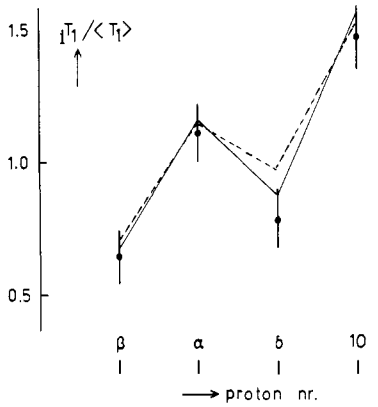

Figure 5. Results of T_1 calculations for the chlorophyll special pair: (—) Shipman–Katz model; (- - -) Fong model; (●) observed.

Dimer Geometries from T_1 Data. SLR times have been determined for the α, β, δ, and 10 protons for all samples (see Table II and Figures 3–5). The absolute T_1 values for the monomer are about twice those for samples 2 and 3. This is what one would expect if the measured T_1 values for these samples are those of dimers, since Stokes–Einstein theory for spherical molecules predicts T_1 to be inversely proportional to the molecular weight.[36]

To calculate T_1 of a particular proton from eq 3, we took into account the contributions of all other protons in the molecule. Methyl groups were treated by replacing them by three protons at the average positions.

Calculations on the molecule pyrimidine with known T_1 data and rotational diffusion constants[15] reproduced the published results, corresponding to a unique set of diffusion coefficients in good agreement with experimental values.

For the monomer and both of the dimers the molecular frame of reference was assumed to be coincident with that of the inertial tensor, calculated from the coordinates of ethyl chlorophyllide *a*.[21] The phytol chain was simulated by a homogeneous rod with a length of 0.85 nm, corresponding to the gyration radius of the chain;[36] its average position with respect to the macrocycle plane was estimated from a space-filling molecular model.

For the Chl *a* monomer, the agreement between experimental and calculated T_1 values is satisfactory (Figure 3). The corresponding elements of tensor $\boldsymbol{D}$ have been collected in Table III.

For (Chl *a*)$_2$ evidence has been presented for a 0.2-nm Mg···ring V keto link,[4b] considerably restricting the range of possible geometries. Assuming that the monomers in (Chl *a*)$_2$ are roughly perpendicular to each other[13] and taking into account the relative orientation of the Mg orbitals and ring V keto lone pairs which are involved in bonding, we can further restrict this range. Figure 4 presents some results of the fit for (Chl *a*)$_2$, assuming a perpendicular geometry with Eulerian angles[36] $\Omega = (90, 90, \gamma)$ with γ and the Mg···O=C$_9$ distance as the variables. This figure also shows the results of T_1 calculations for a nonperpendicular geometry proposed previously.[11,12] The results for this configuration are clearly outside experimental error, and their geometry does not appear to be probable.

Accepting a geometry if and only if *all* calculated values of $_iT_1/\langle T_1\rangle$ are within the experimental error, we conclude that the (Chl *a*)$_2$ dimer has most probably the structure given by $\Omega = (90, 90, 135 \pm 20)$. For the full geometrical description of this geometry and the corresponding elements of tensor $\boldsymbol{D}$, we refer to Table III and Figure 6.

For the Chl *a* SP dimer, two different geometries with parallel macrocycles have been proposed by Fong[10] and by Shipman et al.,[38] corresponding to $\Omega = (0, 0, 180)$ and $\Omega = (0, 180, 180)$, respectively; for these two configurations calculated T_1's are shown in Figure 5. From this figure and Table III, it can be inferred that under our experimental conditions the results are in favor of the Shipman–Katz SP model.[40]

Table III. Results of Proton SLR Calculations on Chl *a* Monomer, Dimer, and Special Pair for the Inertial Tensor I, the Rotational Diffusion Tensor D, and the Geometry of the Dimers ($\vec{V}$, Ω)

	monomer	dimer	SP[b]
geometry[a]			
$\vec{V}$, Å		(7.5, −0.65, 0)	(7.7, −0.13, 3.6)
Ω, deg		(90, 90, 135)	(0, 180, 180)
$10^{43}I_{xx}$, kg m^2	8	20	16
$10^{43}I_{yy}$, kg m^2	1	20	7
$10^{43}I_{zz}$, kg m^2	8	100	20
$10^{-9}D_{xx}$, s^{-1}	5	0.6	0.5
$10^{-9}D_{yy}$, s^{-1}	2	3	0.5
$10^{-9}D_{zz}$, s^{-1}	5	2	3
$10^{-9}\langle D\rangle$, s^{-1}	4	1.9	1.3
Principal Axes[a] of Inertial Diffusion Tensor			
{x}	(1, 0.1, −0.1)	(0.25, −0.43, 0.87)	(0.91, 0, 0.42)
{y}	(−0.1, 1, 0.1)	(0.93, −0.15, −0.34)	(0, 1.00, 0)
{z}	(0.1, −0.1, 1)	(0.28, 0.89, 0.36)	(−0.42, 0, 0.91)

[a] Vectors are expressed relative to the frame of reference presented in Figure 1 and are defined in the text. [b] Results for the optimum geometry, corresponding to the Shipman–Katz model. [c] $\langle D\rangle \equiv (D_{xx} + D_{yy} + D_{zz})/3$.

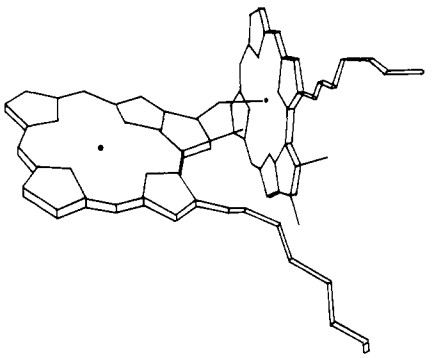

Figure 6. View of (Chl *a*)$_2$ pure dimer; in reality the phytyl chain is longer than indicated here.

Dimer Geometries from Ring-Current Shifts. To be able to relate dimer geometries to ring-current shifts, we first calibrated

(36) Tanford, C. "Physical Chemistry of Macromolecules"; Wiley: New York, 1961.
(37) Goldstein, H. "Classical Mechanics"; Addison-Wesley: London, 1964; pp 107–109.
(38) Shipman, L. L.; Cotton, T. M.; Norris, J. R.; Katz, J. J. *Proc. Natl. Acad. Sci. U.S.A.* **1976**, 1791.

(39) In this context, it is interesting to compare these results with those for a folded, covalently linked pyrochlorophyll dimer (Boxer, S. G.; Closs, G. L. *J. Am. Chem. Soc.* **1976**, *98*, 5406). These authors find that the dimer methine protons have a smaller chemical shift relative to those in the monomer, contrary to our results. Their results point, according to the double-dipole model to a Fong-type dimer structure. This is confirmed by constructing a molecular model of the covalently linked dimer, which demonstrates that folding of the dimer cannot give rise to a configuration of the chlorophyll macrocycles necessary for the formation of the

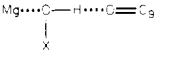

link of the Shipman–Katz structure.

(40) We have studied the SP in an environment described by Cotton,[8a,b] whereas the Fong[10c] dimer is formed with water molecules as ligands and methylcyclohexane as a solvent. Although we do not expect water molecules to behave completely different from ethanol, the combination solvent/ligand may be an important factor determining the detailed structure of the SP.

eq 8 for monomeric Chl *a*. For $\mu_H = 21 \times 10^{-3}$ nm^3 and $\mu_P = 18 \times 10^{-3}$ nm^3, we found optimum agreement between observed and calculated ring-current shifts. In these calculations we have used the shifts of the nuclei α, β, δ and 1, 3, 5;[26] proton 10 cannot be used since no corresponding proton is present in the reference compound (pyrrole). For the (Chl *a*)$_2$ dimer and the special pair, ring-current shifts were calculated with the help of eq 9, varying the dimer geometry. By considering the signs and relative magnitudes of the dimer ring-current shifts relative to the monomer shifts, some conclusions can be drawn about the dimer geometries.

Comparison of the experimental and calculated shifts for (Chl *a*)$_2$ results in the geometry:

$$\vec{V} = (7.5 \pm 0.3, -0.3 \pm 0.7, -0.4 \pm 0.4 \text{ Å})$$

and

$$\Omega = (90 \pm 10°, 90 \pm 10°, 100 \pm 10°)$$

in fair agreement with the results derived from T_1 data and supporting the previous assumption of coinciding axes of inertia and diffusional rotation.

For Chl *a* SP, we note that all experimental dimer ring-current shifts are positive relative to those of the monomer, with the shift of proton 10 being the largest. As in the proton T_1 calculations on the SP, we have only investigated the Fong[10] and the Shipman–Katz[38] SP geometry. All calculated ring-current shifts in the Fong configuration turn out to be negative relative to those of the monomer, whereas in the Shipman–Katz configuration most shifts are positive (Table I), with proton 10 having the largest shift. Thus, also ring-current calculations indicate the Shipman–Katz structure to be the most probable SP geometry.[39]

The finding that both ring-current and SLR results point to the Shipman–Katz structure does not rule out the existence of the Fong SP structure, as the structural details of the dimer may depend on the nature of the solvent and the ligand.[40]

Discussion

We will not discuss whether the main assumptions underlying the calculations of proton relaxation times are valid.

The rotational diffusion condition is met[41] if the ratio between the rotational correlation time $\tau_c = (6D)^{-1}$ and the free rotor time $\tau_f = (2\pi/9)I/kT$ is larger than ~ 5. As follows from Table III both Chl *a* dimers obey this condition, whereas for the monomer additional reorientational mechanisms may be present.

Since dilution of the samples did not change T_1's and all measurements were carried out in fully deuterated solvents, intermolecular dipole–dipole relaxation can be excluded.

The SLR calculations in the previous sections have implicitly assumed that the condition $\omega\tau_c << 1$ is obeyed.

For the dimers, we have only used T_1 data determined at 100 MHz, so that $\omega\tau_c \approx 0.1$, sufficiently small to use the present formalism.

We note that for macroscopic bodies with homogeneous mass distribution in a viscous fluid, the principal axis system of the rotational friction tensor coincides with that of the inertia tensor.[22] To a first approximation, the fairly large chlorophyll molecules may be described by this model: electric dipole solvent–solute interactions are not expected to result in a significant shift of both axis systems,[18,19,42] since the molecular reorientation is controlled by the repulsive parts of the solute–solvent potential, corresponding to a sterically hindered motion, rather than by attractive forces of dipolar or dispersive origin.[15,43] Moreover, it turns out that the relative values of the SLR times remain within their experimental error limits for moderate variations (±15°) in the relative orientation of both axis systems.

Since monomeric Chl *a* is approximately planar, one diffusion axis can be assumed to be perpendicular to the molecular plane. The presence of the phytol chain is expected to introduce some axial symmetry about this chain. The diffusional principal axis system, suggested by these symmetry arguments, is in line with the axis system presented in Table III. For Chl *a* SP, one principal diffusion axis can be unambiguously assigned to its C_2 symmetry axis. For the Shipman–Katz structure, this axis is parallel to *y* (see Table III and Figure 1).

The calculated and experimental ring-current shifts for Chl *a* monomer agree quite well, but for the dimers only the general trends agree (Table I). This is probably due to mutual perturbation of current loops resulting in a change of positions and magnitudes of the equivalent dipoles. Furthermore, some observed protons of one-half of the dimer are situated closely above or below the macrocycle plane of the other half. For these nuclei deviations between predicted and experimental ring-current shifts are expected. Since we have optimized μ_H and μ_P for the monomer, the experimentally observed dimer ring-current shifts are not expected to agree quantitatively with predictions. In view of the simplificity of the double-dipole model, the qualitative agreement obtained is satisfactory.

We conclude that data from two different NMR methods yield very similar geometries for each of the two dimers. Calculations on the excited-state properties of these dimers[44a,b] are also in agreement with these geometries.

Although the calculations of the (Chl *a*)$_2$ dimer geometry using proton SLR data did not show any evidence of multiple minima, we emphasize that with the present experimental accuracy the geometry of the chlorophyll dimers cannot unambiguously be determined from the experimental T_1 data alone, and ring-current calculations are needed as additional independent evidence for the proposed structures.

Rotational Diffusion Constants. The observed average diffusion constant $\langle D \rangle$ of the monomer is found to be approximately twice that of the dimers (Table III), in agreement with the predictions of the Stokes–Einstein model.[36] $\langle D \rangle$ of Chl *a* SP is somewhat smaller than that of the (Chl *a*)$_2$ dimer since SP measurements were carried out at lower temperature and higher solvent viscosity. However, the relative magnitude of the components of tensor $\boldsymbol{D}$ derived from SLR experiments (Table III) does not agree with the predictions of hydrodynamic theory, neither for the monomer nor for either of the dimers, even if the molecular anisotropy is taken into account.[45] This is not too surprising, since the molecules cannot be represented by ellipsoids and the solvent–solute interface can hardly be viewed as continuous and uniform as hydrodynamic theory requires. We must, therefore, conclude that microscopic solvent–solute interactions make a significant contribution to the rotational behavior of the molecule.[17,40,46]

Conclusions

(1) Proton spin lattice relaxation times can be used to investigate geometries of chlorophyll dimers with molecular weight $M_r \lesssim 2000$, provided that the monomeric geometry is known. Ring-current calculations can provide additional data needed for an unambiguous determination of molecular geometries.

(2) Ring current calculations on molecular dimers appear to be a more direct way to study their geometries than the proton SLR method in view of the higher sensitivity to geometrical parameters and the less severe underlying assumptions of the former method.

(3) For the chlorophylls, the hydrodynamic model has only limited potential to rationalize the measured rotational diffusion constants in terms of molecular geometry.

(4) Both proton SLR calculations and ring-current calculations yield geometries for the (Chl *a*)$_2$ dimer and the special pair in solution very similar to those previously reported: the (Chl *a*)$_2$ dimer consists of two molecules that are approximately perpen-

(41) Gillen, K. T.; Noggle, J. H. *J. Chem. Phys.* **1970**, *53*, 801.
(42) Somorjai, R. L.; Deslauriers, R. *J. Am. Chem. Soc.* **1976**, *98*, 6460.
(43) Chandler, D. *Acc. Chem. Res.* **1973**, *7*, 313.
(44) (a) Kooyman, R. P. H.; Schaafsma, T. J. *J. Mol. Struct.* **1980**, *60*, 373. (b) Kooyman, R. P. H. Ph.D. Thesis, Wageningen, 1980.
(45) Shimizu, H. *J. Chem. Phys.* **1964**, *40*, 754.
(46) The hydrodynamic model is essentially macroscopic, approximating the molecule as a solid body moving in a homogeneous, continuous solvent medium. For a large molecules, such as proteins ($M_r \geq 10^5$) this is a reasonable approximation (Tao, T. *Biopolymers* **1969**, *6*, 609).

dicular to each others, whereas under the present experimental conditions the special pair has the Shipman-Katz geometry.

Acknowledgment. We thank P. A. Jager for technical assistance and Dr. G. Jansen and Dr. A. J. Hoff for valuable discussions of this work. We are indebted to Dr. J. Norris for a generous gift of perdeuterated chlorophyll and to Bruker AG, Zürich, for making available their NMR spectrometer for deuterium measurements. This work was supported by the Netherlands Foundation for Chemical Research (S.O.N.) with financial aid from the Netherlands Organization for the Advancement of Pure Research (Z.W.O.).

Registry No. (Chl a)$_2$, 18025-08-6.

Paramagnetic Carbon-13 Shifts Induced by the Free Radical Tempo. 2. Nitrogen Heterocycles

Zu Wen Qui,† David M. Grant,* and Ronald J. Pugmire

Contribution from the Department of Chemistry, University of Utah, Salt Lake City, Utah 84112. *Received July 12, 1982*

Abstract: With use of the free radical Tempo as a shift and relaxation reagent, both paramagnetic shifts and spin-lattice relaxation rates of nitrogen heterocycles are reported. Paramagnetic shifts of these compounds are larger than the corresponding shifts of the aromatic hydrocarbons, indicating a stronger interaction between nitrogen heterocyclic compounds and Tempo. Paramagnetic shifts increase with the number of nitrogen atoms per molecule. For pyridine type compounds, both shift and relaxation data show that the stronger interaction is not at the adjacent positions to the nitrogen atoms. It would appear in these heterocyclic complexes with Tempo that the nitrogen atoms tend to orient away from the N-O group in Tempo. In contrast, imidazole and indole exhibit a much stronger interaction with the Tempo due to hydrogen bond formation, and the positions near the N-H group exhibit larger paramagnetic shifts and relaxation rates. An approximate static model involving an indole-Tempo, hydrogen-bond complex accounts for the relaxation data from which both an equilibrium constant of complexation and a hydrogen-bond distance in the indole-Tempo complex could be estimated.

The relatively stable free radical Tempo has been used[1] in both aromatic and paraffinic hydrocarbons to induce paramagnetic shifts. The greater effectiveness of Tempo as a shift reagent compared with other free radicals was exhibited especially for the aromatic hydrocarbons. As a natural extension, induced spin-lattice relaxation rates along with paramagnetic shifts of ^{13}C in some nitrogen heterocycles are reported in this work. Nitrogen heterocycles are important compounds not only because of their structural similarity with aromatic hydrocarbons but also because of their intermolecular complexation capacity. Nitrogen heterocycles are also significant in the areas of biomedicine[2] and fossil fuels.[3]

The paramagnetic induced shift $\overline{\Delta\delta_f}$, in liquids results[4] from a contact interaction, $\overline{\Delta\delta_f}^{cont}$, and a dipolar interaction, $\overline{\Delta\delta_f}^{dip}$. The direct dipolar interaction between a magnetic moment of an unpaired electron, e, and a magnetic nucleus, N, is inversely proportional to r_{eN}^3, the distance between the free electron and the magnetic nucleus. The theoretical treatment of the pseudocontact term depends, among other things, on the anisotropy of the electron spin g tensor.[5] Hirayama and Honyu have assumed an axially symmetric g tensor in their treatment of Eu and Pr complexes in arriving at relative geometric factors for quinoline, isoquinoline, and acridine.[6] On the other hand, contact interactions arise from a finite unpaired electron spin density in s-type atomic orbitals centered on the nucleus. While the contact interaction is not explicitly distance dependent, it does depend upon the nature of the free radical and its proximity to the affected compound. Direct overlap of a molecular orbital containing the unpaired electron or induced unpaired spin density at the magnetic nucleus via a spin polarization mechanism is required to give an induced shift. Thus, the relative magnitude of these induced shifts at different nuclei within a molecule provide information on the average relative position of the Tempo with respect to the molecule. A quantitative description can only be obtained from an appropriate quantum mechanical calculation if the details of the intermolecular associations are known.

Levy and Komoroski[7] have shown that spin-lattice relaxation data complement paramagnetic shift data. At low concentrations of Tempo the induced shifts and line broadening are relatively small while effects upon the spin-lattice relaxation times (T_1's) are pronounced. The observed relaxation rate, R_1^{obsd}, the inverse of the T_1^{obsd}, is the sum of the various diamagnetic relaxation rates, R_1^{dia}, resulting from dipolar, spin-rotation, scalar, and chemical shift anisotropy mechanisms and from the paramagnetic relaxation rate R_1^e, due to the electron-nuclear relaxation mechanism. When the electron-nuclear dipole-dipole interaction dominates R_1^e, the usual sixth power distance dependence will control the relaxation, and the geometrical relationship between the free radical and the nitrogen heterocycle can be determined. Levy and Komoroski[7] successfully studied the interaction of isoborneol and phenol with $Cr(acac)_2$ and $Fe(acac)_3$. In this study of the indole-Tempo complex, the equilibrium constant and the average distance be-

† On leave from Jilin University, Changchun, Jilin, People's Republic of China.

(1) Qui, Z. W.; Grant, D. M.; Pugmire, R. J. *J. Am. Chem. Soc.* **1982**, *104*, 2747.
(2) Dwek, R. A.; Campbell, I. D.; Richards, R. E. "NMR in Biology"; Academic Press: New York, 1977.
(3) For coal the nitrogen content is usually in the 1-2% range on a moisture- and ash-free basis. Elliott, M. A., Ed. "Chemistry of Coal Utilization"; Wiley-Interscience: New York, 1981; p 28. For crude shale oil the nitrogen content is approximately the same. See, for instance: Fenton, D. M.; Henning, H.; Richardson, R. L. In "Oil Shale Tar Sands and Related Materials"; Stauffer, H. E., Ed.; American Chemical Society: Washington, DC, 1981; ACS Symp. Ser. No. 163; p 315.
(4) LaMar, G. N.; Horrocks, W. DeW; Holm, R. H., Jr. "NMR of Paramagnetic Molecules"; Academic Press: New York, 1973.
(5) Harris, R. K. "Nuclear Magnetic Resonance Spectroscopy"; Pitman Books Limited: London, 1983; p 207.
(6) Hirayama, M.; Honyu, Y. *Bull. Chem. Soc. Jpn.* **1973**, *46*, 2687.
(7) Levy, G. C.; Komoroski, R. A. *J. Am. Chem. Soc.* **1974**, *96*, 678.

0002-7863/84/1506-0557$01.50/0